Modification of interplanetary shocks near the bow shock and through the magnetosheath

J. Šafránková,[1] Z. Němeček ,[1] L. Přech,[1] A. A. Samsonov,[2] A. Koval,[3] and K. Andréeová[1]

Received 27 April 2007; revised 14 May 2007; accepted 21 May 2007; published 21 August 2007.

[1] Fast forward interplanetary (IP) shocks have been identified as a source of the largest geomagnetic disturbances. These shocks can evolve in the solar wind, and they are modified both by interaction with the bow shock and during their propagation through the magnetosheath. Our contribution continues the study of the evolution of IP shocks in the magnetosheath. We compare profiles of the magnetic field and plasma parameters observed in the magnetosheath with profiles of the same parameters predicted by an MHD magnetosheath numerical model. The IP shock transmission into and its propagation through the magnetosheath cause inward and then outward motions of the bow shock, and these motions result in an "indentation" of the bow shock surface. This indentation (trough) flows along the bow shock together with the IP shock. Furthermore, we found that the interaction of the IP shock with the bow shock results in two discontinuities. These effects are consistent with the simulations of the MHD magnetosheath model.

Citation: Šafránková, J., Z. Němeček, L. Přech, A. A. Samsonov, A. Koval, and K. Andréeová (2007), Modification of interplanetary shocks near the bow shock and through the magnetosheath, *J. Geophys. Res.*, *112*, A08212, doi:10.1029/2007JA012503.

1. Introduction

[2] Geomagnetic storms and strong changes of magnetospheric properties due to sudden variations in solar wind conditions affect a wide variety of systems on Earth and in orbit [*Tsurutani and Gonzalez*, 1997]. Interplanetary pressure events, like interplanetary (IP) shocks, compress or expand the magnetosphere and increase or decrease the magnetopause and tail currents that result in changes of other near-Earth current systems [*Collier et al.*, 1998; *Le et al.*, 1998]. The geoeffectiveness of solar wind structures and discontinuities is related to their 3-D geometry and orientation. Since multispacecraft observations are necessary for the determination of the 3-D geometry and structure of shocks and other features in the solar wind [e.g., *Thomsen*, 1988], not too many experimental studies have addressed this problem. Moreover, before IP shocks reach the magnetosphere, they interact with the Earth's bow shock, propagate through the magnetosheath and impinge on the magnetopause; these processes are still poorly understood.

[3] The interaction of IP shocks with Earth's bow shock and their modification through the magnetosheath and magnetopause have been a subject of a quasi-steady gasdynamic numerical modeling (with convected magnetic field) by *Spreiter and Stahara* [1992]. Using the Rankine-Hugoniot conditions, *Dryer et al.* [1967], *Ivanov* [1964], *Dryer* [1973], *Shen and Dryer* [1972], and *Grib et al.* [1979] have shown that the interaction of the IP shock with the bow shock (which is a fast reversed shock) creates three discontinuities: the fast reverse shock (the original bow shock), fast forward shock (the original IP shock) and a contact discontinuity between these shocks in a one-dimensional hydrodynamic case. A comparison between the 3-D MHD simulations and experimental observations was prepared by *Zhuang et al.* [1981] and the authors concluded that all observed discontinuities moved with velocities corresponding to the Rankine-Hugoniot conditions.

[4] In their MHD estimations, *Grib* [1982] and *Pushkar et al.* [1991] found that the interaction of the IP and bow shocks results in a train of different kinds of discontinuities and the number of these discontinuities changes with the distance from the Sun-Earth line (including a complete sequence of seven forward and reverse MHD discontinuities at the magnetospheric flanks). These conclusions were confirmed by the 1-D simulation studies of *Yan and Lee* [1996] that found five discontinuities and a modified bow shock along the Sun-Earth line.

[5] On the other hand, as *Zhuang et al.* [1981] noted, the propagation of IP shocks within the magnetosheath is propagation through an inhomogeneous medium to the obstacle: the magnetopause. Analysis of the Rankine-Hugoniot conditions [*Grib*, 1972; *Grib et al.*, 1979; *Wu*, 2003] shows that the interaction between the fast shock and the magnetopause (defined as a tangential discontinuity) results in a rarefaction wave propagating toward the bow shock. The presence of this wave reflected from the magnetopause was indicated by *Zhuang et al.* [1981].

[6] In the magnetosheath, the predicted discontinuity shape remains nearly planar in the gasdynamic model [*Spreiter and Stahara*, 1994]. This prediction is supported by observations reported by *Szabo* [2005] and *Russell et al.*

[1]Faculty of Mathematics and Physics, Charles University, Prague, Czech Republic.
[2]Institute of Physics, St. Petersburg State University, St. Petersburg, Russia.
[3]NASA Goddard Space Flight Center, Greenbelt, Maryland, USA.

Copyright 2007 by the American Geophysical Union.
0148-0227/07/2007JA012503

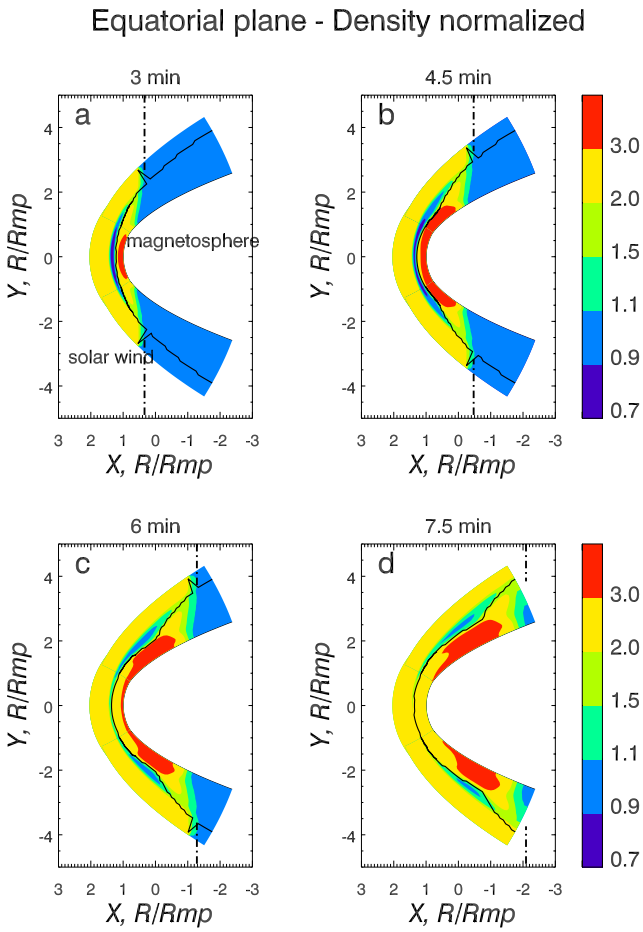

Figure 1. Cross section of the simulation box during passage of a IP shock in the equatorial plane: (a) 3, (b) 4.5, (c) 6, and (d) 7.5 min. The ion density was normalized to its initial values at each point of the box in order to show changes caused by the IP shock propagation. The IP shock location in the solar wind is shown by the dashed-dotted line, and the black curve shows the bow shock position. This position was determined as a place with maximum density gradient. However, this algorithm fails at the place where the IP shock and bow shock meet; thus it produces spikes seen in Figures 1a, 1b, and 1c.

[2000]. On the other hand, deviations from the planarity assumption have been also reported [e.g., *Russell et al.*, 1983; *Šafránková et al.*, 1998; *Szabo et al.*, 2001]. A series of papers by *Koval et al.* [2005, 2006a, 2006b] demonstrates that the shock front in the magnetosheath is inclined and this inclination causes a delay of the shock arrival to the magnetopause. A nonplanar shock propagation through the magnetosheath derived from experimental observations has been confirmed by two numerical MHD simulations [*Koval et al.*, 2006b].

[7] *Samsonov et al.* [2006] simulates the propagation of an IP shock from the supersonic solar wind to the magnetopause using a local 3-D MHD magnetosheath model. An IP shock is assumed to be perpendicular to the solar wind velocity and the angle between the interplanetary magnetic field (IMF) and velocity vectors is equal to 45 degrees. In their 3-D simulations, the interaction of an IP shock with the bow shock results to an inward bow shock motion, it generates new discontinuities propagating through the magnetosheath toward the magnetopause with the plasma flow velocity. Moreover, their numerical model allows them to simulate three different types of magnetopause response: (1) a stationary magnetopause without a response to changes of the upstream pressure, (2) a magnetopause that moves inward with a speed derived from pressure balance, and (3) a magnetopause that moves with a speed estimated from magnetopause location models.

[8] In this paper, we present a series of observations of the interaction of fast forward shocks with the bow shock and their propagation within the magnetosheath and we compare the experimental observations with predictions of different versions of the aforementioned 3-D MHD model.

2. MHD Modeling

2.1. MHD Magnetosheath Model

[9] The numerical model [*Samsonov et al.*, 2006] solves a typical system of the nonstationary MHD equations using the TVD Lax-Friedrichs II-order scheme. It uses a combination of the spherical coordinates in the subsolar region and of the parabolic coordinates on the magnetosheath flanks. The two coordinate systems intersect and the values from inner points of one coordinate system are used to determine the boundary conditions for the other system. The grid spacing applied in the paper is $\approx 0.25\ R_E$. The outer numerical boundary is in the supersonic solar wind. In the initial conditions, we take typical solar wind parameters near 1 AU ($B_1 = 5$ nT, $n_1 = 5$ cm^{-3}, $T_1 = 2 \times 10^5$ K, $v_1 = 400$ km s^{-1}) with the angle between the IMF and solar wind velocity equal to 45° and $B_Z = 0$. Then, we impose an artificial fast forward MHD shock with jump conditions satisfying the Rankine-Hugoniot relations ($B_2/B_1 = 2.25$, $v_2/v_1 = 1.31$, $n_2/n_1 = 2.84$, $v_{sh} = 594$ km s^{-1}, $M_A = 4$). Hereafter, the suffix *sh* is used for IP shock parameters, the suffixes 1 and 2 stand for upstream and downstream parameters of the IP shock, respectively. The symbols are used in accord with their general meaning.

[10] The shock is planar with the normal along the X_{GSM} axis. The bow shock forms inside the numerical field self-consistently in the simulation. The inner boundary corresponds to an impenetrable magnetopause with conditions $v_n = 0$ and $B_n = 0$. This assumption seems to be unrealistic because the pressure jump associated with the IP shock should push the magnetopause inward. However, as *Shen and Dryer* [1972] pointed out, this inward motion can be connected with a plasma depletion in a front of the magnetopause that would stop the inward motion. Thus the magnetopause can even move slightly back on a scale of several minutes. The plasma depletion following the interaction of the IP shock with the magnetopause was interpreted in terms of generation of a rarefaction wave propagating upstream by *Grib et al.* [1979]. Since we are not able to model such complicated magnetopause motion, we think that the stationary magnetopause can be taken as a first rough approximation. The other conditions of the magnetopause response to upstream changes and their implementation into the model will be discussed later.

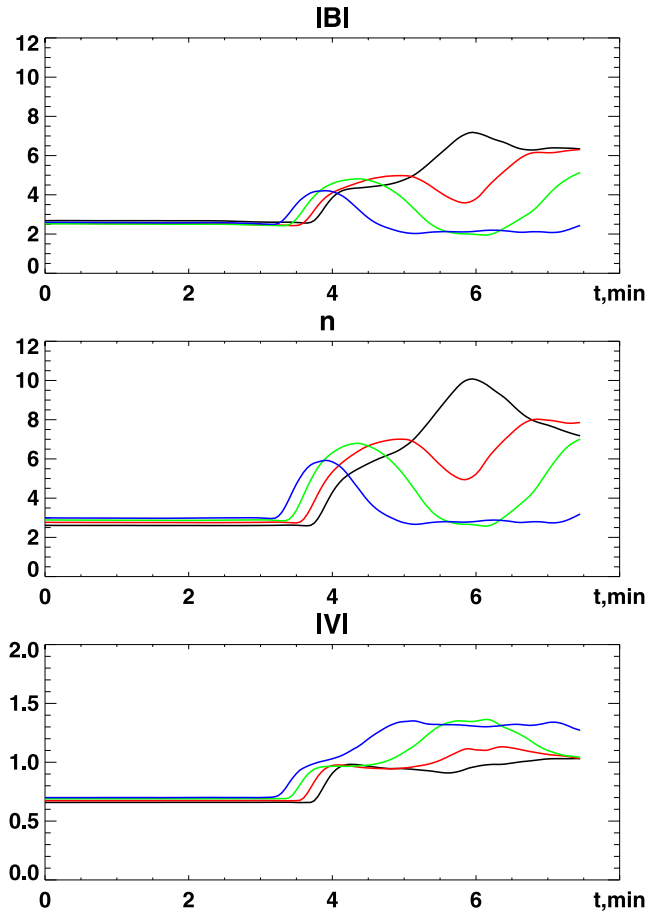

Figure 2. Simulated profiles of the magnetic field magnitude, density, and velocity as would be observed by the spacecraft distributed along the Z_{GSM} axis at 18.5 R_E (black), 19 R_E (red), 19.5 R_E (green), and 20 R_E (blue), assuming the subsolar magnetopause at $X = 10$ R_E.

2.2. Cross Section of the Interaction Region

[11] Figure 1 shows contours of the ion density in the equatorial plane. An IP shock was launched at $t = 0$ and its location is shown by the dashed-dotted lines in Figures 1a–1d. Approximately 1.5 min later, the IP shock interacts with the bow shock that starts to move inward. We should note that this inward motion is a consequence of changed magnetosheath parameters because no information about the IP shock reached the magnetopause before $t = 3$ min (Figure 1a). However, magnetosheath parameters further evolve and this evolution leads to outward bow shock motion in the simulation at $t > 6$ min (Figures 1c and 1d). Note that this outward motion should be taken with a care because the (impenetrable) magnetopause does not react to the increase of the upstream pressure in this particular model run.

[12] A very interesting feature is a trough occurring on the bow shock surface. This trough creates a ring around the Sun-Earth line because it can be seen in both equatorial and meridional (not shown) cross sections. The trough proceeds along the bow shock surface with a slightly smaller speed than that of the original IP shock. The motion of the trough would result in multiple bow shock crossings of the spacecraft in an appropriate location. A comparison of the meridional and equatorial cross sections shows that, although the magnetosheath is not axisymmetric in the model because of the IMF draping, this asymmetry does not influence the IP shock propagation and bow shock deformation substantially.

2.3. Temporal Profiles

[13] The map in Figure 1 provides an overview of the whole interaction process but it cannot be compared with observations directly. For this reason, we have plotted temporal profiles as would be seen by a spacecraft at different magnetosheath locations. The curves in Figure 2 show such profiles at four distances from the magnetopause along the Z_{GSM} axis. We have chosen these locations because IP shock observations at the Sun-Earth line are rather rare. Figure 2 reveals that these profiles are very sensitive to the actual spacecraft location. The spacecraft at the black position would observe a two-step front of the IP shock in the magnetosheath. The separation of steps is $\approx$1.5 min. The spacecraft located a little farther from the magnetopause (red line) would observe a shock approximately at the same time but a depletion would be observed instead of the second front. On the other hand, the spacecraft nearer the bow shock would see the IP shock passage in the magnetosheath but one or 2 min later it would cross the bow shock and enter the solar wind for several minutes. The duration of solar wind intervals increases at 19.5 R_E from the magnetopause (green). This short-time visit into the solar wind is a consequence of the already mentioned motion of a trough along the bow shock surface. The last profile (blue) shows that an observer near the bow shock would register the IP shock in the magnetosheath followed by an exit of the spacecraft into the solar wind a little later. We should point out that reentry of the spacecraft into the magnetosheath predicted by the model will be not necessarily observed because a compression of the magnetopause is not self-consistently introduced.

2.4. Influence of the Magnetopause Response on Model Results

[14] Since the modeling of IP shock interactions with the bow shock is thoroughly discussed by *Samsonov et al.* [2006], we will concentrate here on those features that can be compared with the experiment. The comparison can be divided into two parts: (1) observations of the IP shock itself and (2) later phases of the interaction process. This division is important from the model point of view. The first phase does not depend on the magnetopause reaction and a modification of the IP shock is a result of its interaction with the bow shock. This interaction creates a new discontinuity that would follow the IP shock. This discontinuity was identified as a combination of a forward slow expansion wave, a contact discontinuity, and reverse slow shock [*Samsonov et al.*, 2006]. Since all these discontinuities are created simultaneously and their propagation speeds are very similar, they cannot be distinguished in the model as well as in experimental data. Consequently, the model predicts that the spacecraft in the magnetosheath on the Sun-Earth line would observe the modified IP shock characterized by an increase of the density, temperature, velocity, and magnetic field. This shock will be followed by another discontinuity that would exhibit nearly the same

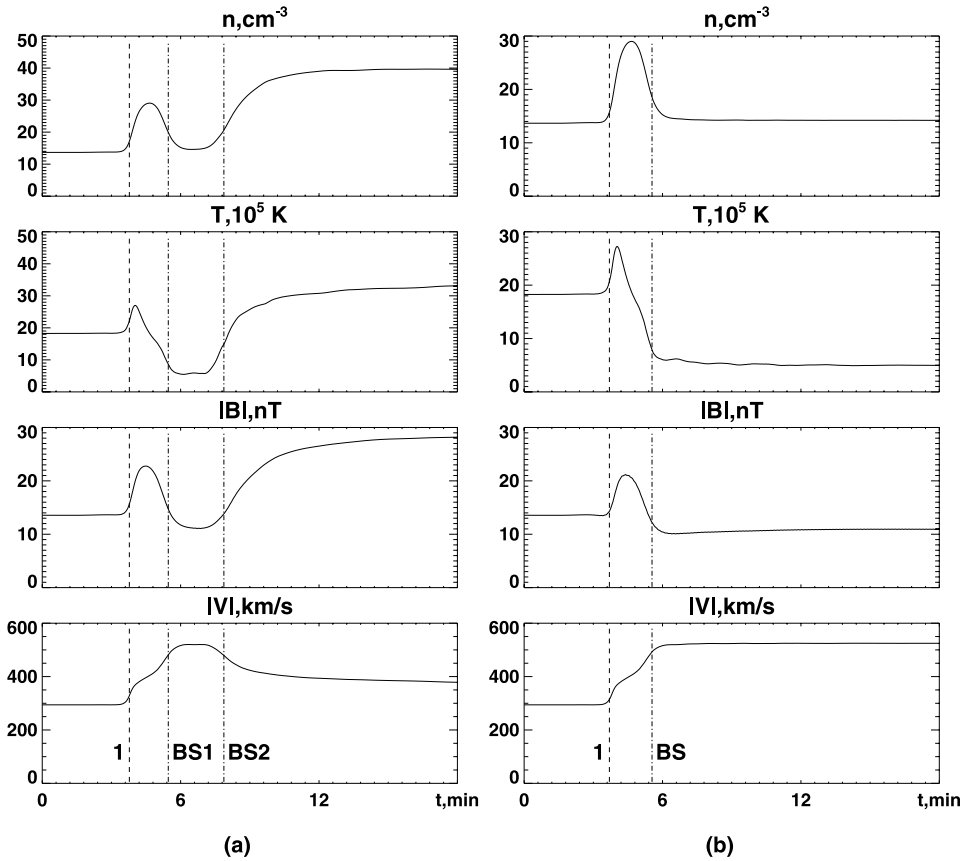

Figure 3. Simulated profiles of the density, temperature, magnetic field magnitude, and velocity with different reaction of the magnetopause: (a) run with a standing magnetopause and (b) run with the magnetopause moving inward with a speed of $\approx$100 km s^{-1}. The vertical lines denote the following: 1, IP shock; BS1, first bow shock crossing; and BS2, second bow shock crossing.

increase of the density but a decrease of the temperature, whereas the velocity and magnetic field remain nearly unchanged and only the magnetic field slightly increases at the Sun-Earth line. The temporal separation of these two discontinuities in the observations would depend on the location of the spacecraft in the magnetosheath. It can be several seconds near the bow shock but it can reach $\approx$1 min in the magnetopause region. However, it should be pointed out that the jumps of parameters across the original IP shock in the solar wind are larger than those in the magnetosheath.

[15] In the later phase, these discontinuities reach the magnetopause and the model results strongly depend on its reaction. If no or slow ($\approx$100 km s^{-1}) reaction is expected, a fast reverse shock will propagate upstream, however, a rarefaction wave would be observed in the case of a very fast ($\approx$200 km s^{-1}) inward magnetopause motion [*Samsonov et al.*, 2006]. As noted there, the presence of the reflected fast expansion wave follows also from an analysis of Rankine-Hugoniot relations [*Grib et al.*, 1979].

[16] The magnetosheath parameters downstream of the IP shock are modified and this modification causes an inward motion of the bow shock. The reflected wave propagated from the magnetopause would further modify the magnetosheath parameters and this modification would result in a new bow shock displacement. Since the runs in the work of *Samsonov et al.* [2006] are too short to see this effect and all their plots show the Sun-Earth line and our observations are located near the flanks, we made a new run of the *Samsonov et al.* [2006] model in which we concentrate on modification of magnetosheath parameters. We put an artificial spacecraft on the Z_{GSM} axis near the bow shock and the predicted profiles of basic parameters are plotted in Figure 3 for two runs: (1) run with a standing magnetopause (Figure 3a) and (2) run with the magnetopause moving inward (Figure 3b) with a speed of $\approx$100 km s^{-1}. This speed seems to be realistic for a sharp increase of the upstream pressure and it is consistent with our preliminary analysis of the same IP shock using the BATS-R-US global model (not shown). Although the runs use an increased spatial resolution (grid spacing is 400 km in this case), the basic observational features in Figure 3 are very similar to those in Figure 2. The spacecraft would observe the IP shock in the magnetosheath and then it would cross the bow shock because of its inward motion. The modification of the magnetosheath parameters by the reverse shock reflected from the standing magnetopause results in the bow shock outward motion that is recorded as a consecutive bow shock crossing. On the other hand, if the magnetopause reaction to the pressure jump is allowed (Figure 3b), the outward bow shock displacement is not observed and the spacecraft remains in the solar wind.

Table 1. Locations of the Spacecraft During Presented Events[a]

		GSE Location of Spacecraft			
Spacecraft	Figure	X, R_E	Y, R_E	Z, R_E	Time, UT
Wind	4	131.9	2.3	9.1	2332
Interball-1	4	−4.5	19.9	−15.4	2352
Wind	5	179.3	16.5	−3.6	1213
Geotail	5	3.9	14.2	0.8	1306
Wind	6	234.7	−17.8	−27.4	1102
Interball-1	6	2.6	18.6	−10.7	1159
Wind	7	92.1	8.7	−3.0	0715
Geotail	7	4.7	15.9	1.5	0735

[a]The time denotes approximately the times of an IP shock observation by a particular spacecraft.

[17] It should be noted that other discontinuities generated by the bow shock–IP shock interaction [*Samsonov et al.*, 2006] are not seen in Figure 3, probably because our artificial spacecraft is located close to the bow shock and the temporal separation of the discontinuities from the IP shock front is too small. Nevertheless, a careful inspection of density and temperature profiles given in Figure 3 shows that the temperature peaks earlier than the density. This suggests that the IP shock front consists of two parts. The first part is characterized by the simultaneous increasing of the density and temperature, whereas the rise of the density is accompanied with the temperature drop in the second part. We think that the first part is the original IP shock and the second part can be considered as the discontinuity resulting from the IP shock–bow shock interaction.

3. Observations of IP Shocks in the Magnetosheath

[18] The numerical model predicts several different profiles that could be observed in the magnetosheath and we will check whether this prediction is consistent with the observations. Since bow shock crossings can be easily identified in the spacecraft data, we devote the first subsection to this point. The second subsection deals with a more detail analysis of observed discontinuities.

[19] The Wind spacecraft was used as a solar wind monitor in all presented cases. The magnetosheath data were provided by Interball-1 or Geotail at locations given in Table 1. The events are marked by the number of the corresponding figure that presents the observations. As can be seen from the table, a qualitative comparison of experimental data and model at $X = 0$ is possible.

3.1. Bow Shock Response to the IP Shock Passage

[20] Figure 4 shows an IP shock that was registered by four spacecraft (ACE, SOHO Wind, IMP 8) in the solar wind and by Interball-1 in the magnetosheath on February 11, 2000. The parameters of the IP shock are derived from the timing of observations and they are given in the Figure 4 caption. The Wind solar wind observations are lagged to match the IP shock in the magnetosheath.

[21] Interball-1 observations roughly resemble the features that are shown in blue in Figure 2. The spacecraft was in the magnetosheath and at 2354 UT it observed the IP shock arrival characterized by a sharp increases of the magnetic field strength from 20 to 40 nT and of the ion flux from 3 to 15 × 10^8 cm^{-2} s^{-1}. About 156 s later, the spacecraft crossed the bow shock and entered the solar wind. The time delay between the IP shock and bow shock crossing is larger than the prediction of the model in Figure 3 but the observations were made at $X_{GSE} \approx -5\ R_E$ and thus we can expect only a qualitative agreement. The shock front in the magnetosheath is split into two steps lagged by ≈60 s. The steps are indicated by vertical lines but this feature will be discussed in the next section.

[22] Another example of the IP shock observations in the magnetosheath is shown in Figure 5. The shock was registered by Wind at ≈1214 UT on 28 July 1996. Unfortunately, no other spacecraft was in the solar wind and thus the shock parameter determination is based on the Rankine-Hugoniot relations and the Wind data. However, we note that the predicted time of the shock propagation from Wind to Geotail was 50 min, whereas that observed was 52 min. A good match of these two times suggests that the shock parameters given in the Figure 5 caption were determined properly. Plasma parameters onboard Geotail were measured by two devices. Since their data on the ion density differ, we are showing both values in Figure 5. Our comparison is only qualitative, thus we do not comment these differences.

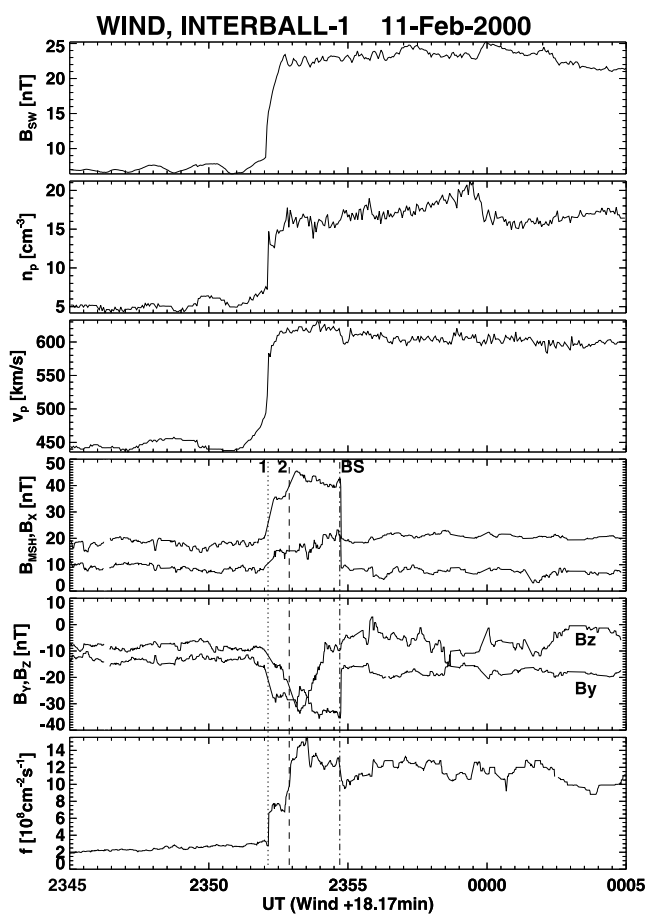

Figure 4. Strong fast forward shock observed on 11 February 2000 by four spacecraft in the solar wind and by Interball-1 in the magnetosheath. Shock parameters are v_{sh} = 577 km s^{-1}, M_A = 3.16, and **n** = [−0.83, −0.35, −0.43]. The normal and speed were computed from timing of four spacecraft observations in the solar wind [*Koval et al.*, 2005].

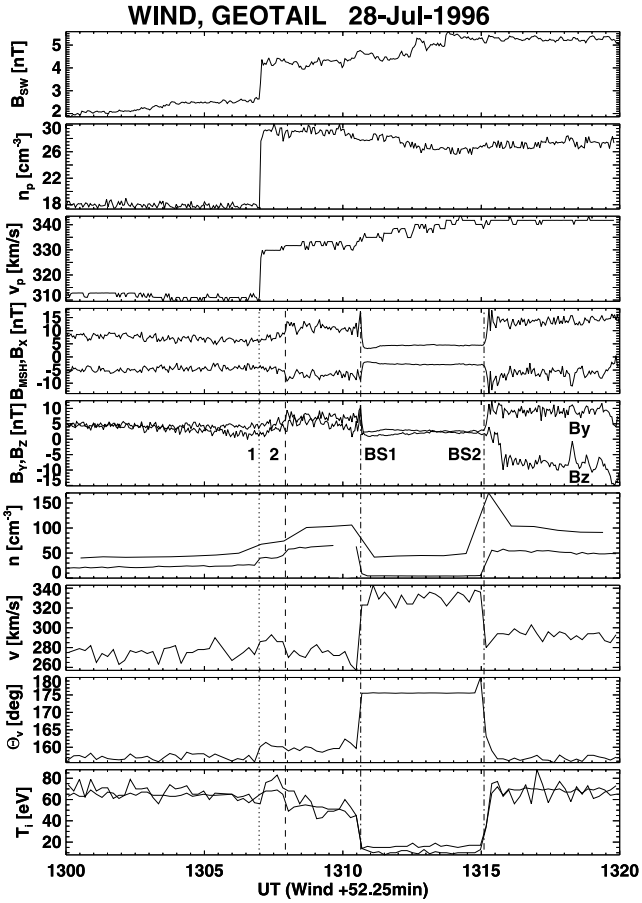

Figure 5. Geotail observations of the IP shock in the magnetosheath on 28 July 1996. The first three plots show Wind solar wind parameters for the sake of reference. The shock parameters in the solar wind are v_{sh} = 339 km s^{-1}, M_A = 2.06, and $\mathbf{n}$ = [−0.92, −0.06, −0.39]. The normals to bow shock crossings are $\mathbf{n}_{1BS1}$ = [0.39, −0.26, 0.88] and $\mathbf{n}_{2BS1}$ = [0.15, 0.04, −0.99].

[23] IP shock observations in the magnetosheath are characterized by an increase of the ion density and a very small increase of the velocity accomplished with a change of its direction characterized by the cone angle, Θ_v in Figure 5. The IP shock is denoted by the vertical dotted line (labeled 1) in Figure 5. The shock is followed (with a delay of ≈55 s) by another discontinuity denoted by the dashed line (labeled 2) in Figure 5. This discontinuity does not possess the character of a fast wave and we will discuss its origin later.

[24] The changes of the magnetic field are gradual but the ratio between preshock and postshock magnetic fields is about 1.6, similar to that observed in the solar wind. The most distinct feature in the Geotail data is short-time excursion (≈260 s) into the solar wind that follows the IP shock front with a delay of about 220 s. This feature is similar to the profile in Figure 3a. The time delays are a little larger but we would like to note that the analyzed event was characterized by a very low solar wind speed and low Mach number. Consequently, one can expect that the timescales would be larger than those in the model (the shock speed in the numerical simulations (Figure 2) was ≈600 km s^{-1} but was ≈340 km s^{-1} in the analyzed case).

[25] The features shown in Figure 5 are very typical. Figure 6 shows another example of an IP shock recorded by ACE and Wind on 4 March 1998 in the solar wind and an hour later by Interball-1 in the magnetosheath. The shock normal computed from the Wind data (see Figure 6 caption) is nearly aligned with the solar wind and the predicted time lags from Wind–Interball-1 (55 min) and from ACE–Interball-1 (66 min) of shock passages match well with the observations. Since IMF B_X is the major IMF component in the preshock interval, the whole dayside magnetosheath is behind the quasiparallel bow shock and magnetosheath observations are rather noisy. Nevertheless, the IP shock front can be clearly identified in the ion flux data. The increase of the magnetic field at the IP front is not distinct but is present. The IP shock front could be structured but we attribute the structures in the ion flux to magnetosheath fluctuations. The IP shock is followed by a pair of bow shock crossings. The relative timing of these crossings with respect to the IP shock is ≈260 s for the first

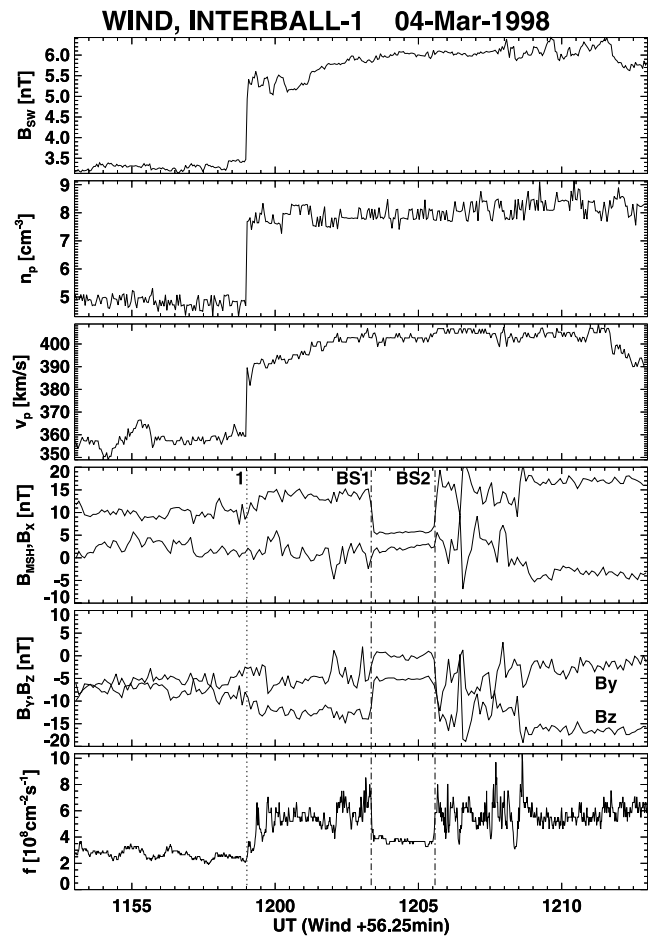

Figure 6. Interball-1 observations of an IP shock in the magnetosheath on 4 March 1998. The shock parameters in the solar wind are v_{sh} = 442 km s^{-1}, M_A = 3.3, and $\mathbf{n}$ = [−0.96, −0.06, 0.29]. The vertical dotted line corresponds to the shock front in the magnetosheath (Interball-1); two dotted-dashed lines indicate two bow shock crossings. The bow shock normals corresponding to these bow shock crossings *BS*1 and *BS*2 are $\mathbf{n}_1$ = [0.78, 0.53, −0.34] and $\mathbf{n}_2$ = [0.62, 0.70, −0.36], respectively.

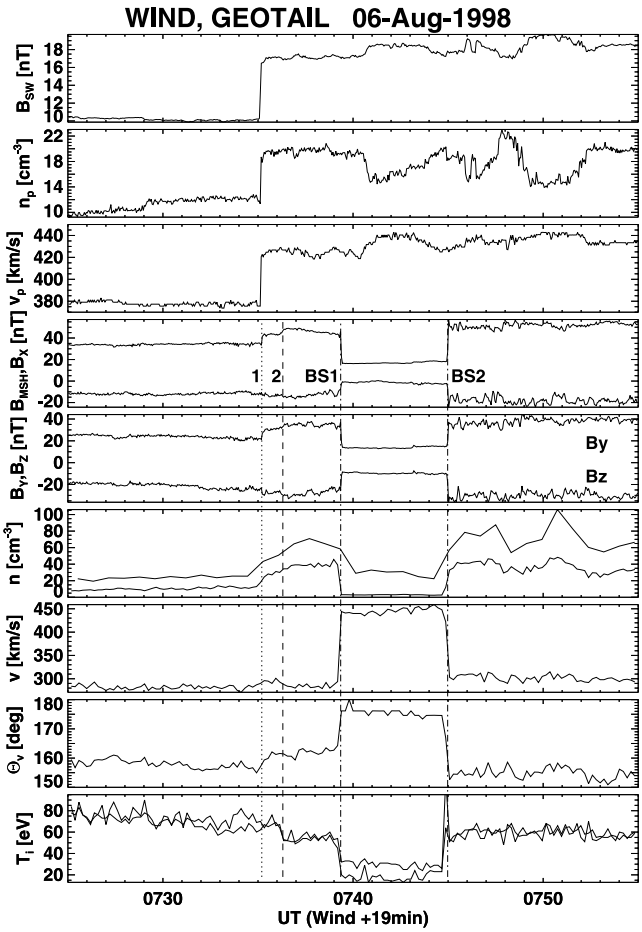

Figure 7. IP shock observed in the magnetosheath by Geotail on 6 August 1998. The shock parameters in the solar wind are $v_{sh} = 489$ km s^{-1}, $M_A = 1.94$, and $\mathbf{n} = [-0.97, -0.11, 0.23]$. The bow shock normals are $\mathbf{n} = [-0.94, -0.32, 0.09]$ and $\mathbf{n} = [-0.73, -0.66, -0.17]$.

crossing and ≈395 s for the second one. Taking into account the solar wind and shock speeds, these delays are qualitatively consistent with the profile given in Figure 3a.

[26] We stress that the observed bow shock crossings in Figures 5 and 6 are a product of the IP shock–magnetosphere interaction because there are no changes in the upstream dynamic pressure or IMF that could cause them. Figure 1 shows a trough propagating along the bow shock surface that could cause the observed crossings. If this trough was passing the spacecraft, the bow shock normal at the first crossing should be inclined toward the Sun-Earth line more than that for the second crossing. Calculated normals for the bow shock crossings shown in Figures 5, 6, and 7 are given in the captions of Figures 5, 6, and 7 and we note that the X component of the normal computed for the first crossing is larger than that for second crossing in both events. This fact suggests that the global features of the interaction are described rather well by our simplified model.

3.2. IP Shock and Associated Discontinuities in the Magnetosheath

[27] As we have pointed out during our previous analysis of global features of the IP shock–magnetosphere interaction, the splitting of the IP shock front into the two-step structure can be frequently observed. The time lag between these steps is of the order of minute. *Samsonov et al.* [2006] suggested that such profile can result from the IP shock–bow shock interaction. On the other hand, reflection of a fast shock from the magnetopause can provide a similar profile of parameters in some magnetosheath locations.

[28] In order to determine the role of the magnetopause, we will analyze two events in more detail. We should point out that this task is difficult because the plasma data usually have an insufficient time resolution and the data on the speed and temperature are not too reliable near sharp fronts. The event on 28 July 1996 (Figure 5) was already discussed, but here we will concentrate on the front itself. The first jump of the ion density from ≈30 cm^{-3} to 40 cm^{-3} (thinner line in the density plot in Figure 5) is similar to that observed in the solar wind. This density jump is accompanied with an increase of the velocity and temperature. It is difficult to identify a corresponding change in the magnetic field strength because of magnetosheath fluctuations, but a gradual rise was observed starting at the density jump. The second increase of the density, up to ≈60 cm^{-3}, is complemented by a small increase of the velocity, a drop of the temperature, and a sharp increase of the magnetic field. Assuming that the first (expected) increase of the magnetic field is masked by magnetosheath fluctuations, the first discontinuity can be classified as a fast forward shock. The second density jump cannot be attributed to any simple MHD discontinuity because the compression of the plasma and field is accompanied with the temperature drop.

[29] Figure 7 presents an other example of a magnetosheath IP shock in the same format as Figure 5. The time resolution of the plasma data is poor but the two-step structure of the front can be identified. The behavior of plasma parameters is the same as in the previous example; the magnetic field exhibits jumps that (within the resolution of plasma data) coincide with the increase of the density. Note that the velocity does not notably change across the second discontinuity. We think that in both examples, the first discontinuity can be classified as a fast forward shock, whereas the second one is probably a combination of several discontinuities that cannot be identified separately because of the time resolution of the data. The most probable interpretation of these observations is that the split front of the discontinuity results from the IP and bow shock interaction and that the second density increase can be attributed to the combination of the forward slow expansion wave, contact discontinuity, and reverse slow shock as suggested by *Samsonov et al.* [2006].

4. Discussion of Model and Experimental Results

[30] The analysis of the observations of the interaction of IP shocks with the bow shock and magnetopause reveals that it is a rather complex task because of the dynamics of a whole region and because of variations of all parameters. In order to simplify it, we can start with the flow around a solid obstacle. During the first minute after the IP shock arrival to the bow shock (prior to the pressure jump arrivals at the magnetopause), the magnetopause is stationary. Information about the magnetopause response to the IP shock arrival

should propagate upstream toward the bow shock against the magnetosheath flow. Thus one would expect a much larger delay in observations of this response in the bow shock region. Since all presented examples were observed near the bow shock, the 1-min separation of two discontinuities excludes the IP shock interaction with the magnetopause as a possible cause of the IP shock front splitting. The model shows such splitting due to the IP and bow shock interaction at the Sun-Earth line [*Samsonov et al.*, 2006]. We think that the fact that the model does not simulate such splitting at the flank (Figure 3) can be attributed rather to insufficiency of the model.

[31] The bow shock location is given by the magnetosheath thickness which is a function of the Mach number and thus the equilibrium bow shock should be located closer to the obstacle after an IP shock passage. Consequently, the MHD model shows inward bow shock motion that can result in a bow shock crossing (Figure 2) and such crossings are observed (BS in Figure 4 and BS1 in Figures 5–7). We would like to emphasize that this bow shock crossing is a consequence of changed upstream parameters and will be present regardless of the magnetopause reaction.

[32] The interpretation of the consecutive bow shock crossings (BS2 in Figures 5–7) is more difficult. We have shown that the observations are consistent with the numerical model that uses a solid magnetopause (Figures 1, 2, 3a) but this model version is clearly oversimplified. However, the model versions applying the realistic magnetopause response do not predict the outward bow shock motion that is observed. On the other hand, this motion is a consequence of a fast shock reflected from the standing magnetopause and we cannot exclude that such reflection can occur at another magnetosphere boundary.

5. Conclusion

[33] We have analyzed a few observations of IP shocks in the magnetosheath. Our analysis is supported by MHD modeling. Attention was devoted to global features of the IP shock–bow shock–magnetopause interaction as well as to the structure of the IP shock front in the magnetosheath. The results of our analysis can be written as follows:

[34] 1. The IP shock passage into the magnetosheath causes the inward motion of the bow shock. This motion is a result of changes of magnetosheath parameters downstream of the IP shock. These observations are in an agreement with the predictions based on the Rankine-Hugoniot conditions [*Grib et al.*, 1979; *Zhuang et al.*, 1981].

[35] 2. The inward bow shock displacement is followed by an outward motion. A combination of these two motions results in creation of an indentation of the bow surface that moves along the bow shock together with the IP shock. The deepness of this indentation should be units of R_E because its motion is very often recorded as two bow shock crossings separated by 1–5 min.

[36] 3. The outward bow shock motion is probably a consequence of the IP shock interaction with an obstacle. This obstacle can be the magnetopause or other boundary in the inner magnetosphere.

[37] 4. The interaction of the IP shock with the bow shock and magnetopause frequently results in two discontinuities. The time lag between them is of the order of 1 min. The first usually exhibits features of the original fast forward shock. The second discontinuity is characterized by a density increase and a decrease of the temperature. The velocity exhibits no or very small change across the discontinuity. The magnetic field magnitude remains nearly unchanged in some cases but in other cases, sharp and large increases are observed.

[38] 5. The discontinuities are products of the IP shock–bow shock interaction and the observed patterns are generally consistent with the MHD magnetosheath model of *Samsonov et al.* [2006].

[39] We were not able to identify more than one discontinuity following the IP shock in the magnetosheath. The train of discontinuities suggested by *Grib* [1982] or *Yan and Lee* [1996] probably could not be observed because, as *Samsonov et al.* [2006] noted, their velocities are very similar and thus they cannot be distinguished in experimental data.

[40] The experimental data are generally consistent with the *Samsonov et al.* [2006] model but several points are still waiting for explanation:

[41] 1. Why does the model not reproduce the observed splitting of the IP shock at the flanks?

[42] 2. What is the source of the outward bow shock motion?

[43] 3. What is the role of the IMF orientation in the IP shock interaction with the bow shock and magnetopause?

[44] The answers to these questions require further effort in modeling and careful analysis of new observations. Of course, many attempts to answer these and related questions were made in course of years. For example, *Shen and Dryer* [1972] and *Grib et al.* [1979] suggested an oscillatory motion of the magnetopause because its interaction with the IP shock could explain observed outward motion of the bow shock. However, these calculations were 1-D and thus they can be probably applied to the subsolar region but our observations were made on the flanks.

[45] **Acknowledgments.** The authors acknowledge the working group at CCMC for model runs. The present work was supported partly by the Research Plane of Ministry of Education of Czech Republic under contract MSM 0026120860 and partly by the Czech Grant Agency under contracts 205/07/0694, 205/06/0875, and 202/03/H162. Their financial support is greatly appreciated. Moreover, K. Andreeova thanks Charles University for grant 147307.

[46] Zuyin Pu thanks Murray Dryer and another reviewer for their assistance in evaluating this paper.

References

Collier, M. R., J. A. Slavin, R. P. Lepping, A. Szabo, and K. Ogilvie (1998), Timing accuracy for the simple planar propagation of magnetic field structures in the solar wind, *Geophys. Res. Lett.*, *25*, 2509–2512.

Dryer, M. (1973), Bow shock and its interaction with interplanetary shocks, *Radio Sci.*, *8*, 893–901.

Dryer, M., D. L. Merritt, and P. M. Aronson (1967), Interaction of a plasma cloud with the Earth's magnetosphere, *J. Geophys. Res.*, *72*, 2955–2962.

Grib, S. A. (1972), The interaction of solar wind shock waves with the magnetosphere of the Earth, *Rep. Beloruss. Acad. Sci.*, *16*(6), 493–496.

Grib, S. A. (1982), Interaction of non-perpendicular/parallel solar wind shock waves with the Earth's magnetosphere, *Space Sci. Rev.*, *32*, 43–48.

Grib, S. A., B. E. Briunelli, M. Dryer, and W.-W. Shen (1979), Interaction of interplanetary shock waves with the bow shock-magnetopause system, *J. Geophys. Res.*, *84*, 5907–5921.

Ivanov, K. G. (1964), Interaction of running shock waves with strong discontinuities in the space vicinity of the Earth, *Geomagn. Aeron.*, *4*, 803–806.

Koval, A., J. Šafránková, Z. Němeček, L. Přech, A. A. Samsonov, and J. D. Richardson (2005), Deformation of interplanetary shock fronts in the magnetosheath, *Geophys. Res. Lett.*, *32*, L15101, doi:10.1029/2005GL023009.

Koval, A., J. Šafránková, Z. Němeček, and L. Přech (2006a), Propagation of interplanetary shocks through the solar wind and magnetosheath, *Adv. Space Res.*, *38*, 552–558, doi:10.1016/j.asr.2006.05.023.

Koval, A., J. Šafránková, Z. Němeček, A. A. Samsonov, L. Přech, J. D. Richardson, and M. Hayosh (2006b), Interplanetary shock in the magnetosheath: Comparison of experimental data with MHD modeling, *Geophys. Res. Lett.*, *33*, L11102, doi:10.1029/2006GL025707.

Le, G., C. T. Russell, and J. G. Luhmann (1998), POLAR magnetic observations of the low-altitude magnetosphere during the January 1997 coronal mass ejection/magnetic cloud event, *Geophys. Res. Lett.*, *25*, 2533–2536.

Pushkar, E. A., A. A. Barmin, and S. A. Grib (1991), MHD-approximation study of the incidence of the solar wind shock on the Earth's bow shock, *Geomagn. Aeron.*, *31*, 522–525.

Russell, C. T., J. T. Gosling, R. D. Zwickl, and E. J. Smith (1983), Multiple spacecraft observations of interplanetary shocks ISEE three-dimensional plasma measurements, *J. Geophys. Res.*, *88*, 9941–9947.

Russell, C. T., et al. (2000), The interplanetary shock of September 24, 1998: Arrival at Earth, *J. Geophys. Res.*, *105*, 25,143–25,154.

Samsonov, A. A., Z. Němeček, and J. Šafránková (2006), Numerical MHD modeling of propagation of interplanetary shock through the magnetosheath, *J. Geophys. Res.*, *111*, A08210, doi:10.1029/2005JA011537.

Shen, W.-W., and M. Dryer (1972), Magnetohydrodynamic theory for the interaction of an interplanetary double-shock ensemble with the Earth's bow shock, *J. Geophys. Res.*, *77*, 4627–4644.

Spreiter, J. R., and S. S. Stahara (1992), Computer modeling of solar wind interaction with Venus and Mars, in *Venus and Mars: Atmospheres, Ionospheres and Solar Wind Interactions*, *Geophys. Monogr. Ser.*, vol. 66, edited by J. G. Luhmann, M. Tatrallyay, and R. O. Pepin, pp. 345–383, AGU, Washington, D. C.

Spreiter, J. R., and S. S. Stahara (1994), Gasdynamic and magnetohydrodynamic modeling of the magnetosheath: A tutorial, *Adv. Space Res.*, *14*(7), 5–19, doi:10.1016/0273-1177(94)90042-6.

Szabo, A. (2005), Interplanetary discontinuities and shocks in the Earth's magnetosheath, in *Multiscale Processes in the Earth's Magnetosphere: From Interball to Cluster*, *NATO Sci. Ser.*, vol. 178, edited by J.-A. Sauvaud and Z. Němeček, pp. 57–71, doi:10.1007/1-4020-2768-0_4, Springer, New York.

Szabo, A., R. P. Lepping, J. Merka, C. W. Smith, and R. M. Skoug (2001), The evolution of interplanetary shocks driven by magnetic clouds, in *Solar Encounter: Proceedings of the First Solar Orbiter Workshop*, edited by B. Battrick et al., *Eur. Space Agency, Spec. Publ.*, *ESA-493*, 383–387.

Thomsen, M. F. (1988), Multi-spacecraft observations of collisionless shocks, *Adv. Space Res.*, *8*(9), 157–166, doi:10.1016/0273-1177(88)90126-3.

Tsurutani, B. T., and W. D. Gonzalez (1997), The interplanetary causes of magnetic storms: A review, in *Magnetic Storms*, *Geophys. Monogr. Ser.*, vol. 98, edited by B. T. Tsurutani et al., pp. 77–90, AGU, Washington, D. C.

Šafránková, J., Z. Němeček, L. Přech, G. Zastenker, K. I. Paularena, N. Nikolaeva, M. Nozdrachev, A. Skalsky, and T. Mukai (1998), The January 10–11, 1997 magnetic cloud: Multipoint measurements, *Geophys. Res. Lett.*, *25*, 2549–2552.

Wu, C. C. (2003), Shock wave interaction with the magnetopause, *Space Sci. Rev.*, *107*, 219–226, doi:10.1023/A:1025588125794.

Yan, M., and L. C. Lee (1996), Interaction of interplanetary shocks and rotational discontinuities with the Earth's bow shock, *J. Geophys. Res.*, *101*, 4835–4848.

Zhuang, H. C., C. T. Russell, E. J. Smith, and J. T. Gosling (1981), Three-dimensional interaction of interplanetary shock waves with the bow shock and magnetopause: A comparison of theory with ISEE observations, *J. Geophys. Res.*, *86*, 5590–5600.

K. Andréeová, Z. Němeček, L. Přech, and J. Šafránková, Faculty of Mathematics and Physics, Charles University, V Holesovickach 2, 18000 Praha 8, Czech Republic. (zdenek.nemecek@mff.cuni.cz; jana.safrankova@mff.cuni.cz)

A. Koval, NASA Goddard Space Flight Center, Greenbelt, MD 20771, USA.

A. A. Samsonov, Department of Earth Physics, Institute of Physics, St. Petersburg State University, St. Petersburg 198504, Russia.